A facile approach for estimating radio-frequency field strength of low-receptivity nuclei

Nghia Tuan Duong, Stéphane Viel, Fabio Ziarelli, Pierre Thureau, Giulia Mollica

A facile approach for estimating radio-frequency field strength of low-receptivity nuclei

Nghia Tuan Duong[a]*, Stéphane Viel[a,b], Fabio Ziarelli[c], Pierre Thureau[a], and Giulia Mollica[a]

[a] Aix Marseille Univ, CNRS, ICR, Marseille, France

[b] Institut Universitaire de France, Paris, France

[c] Aix Marseille Univ, CNRS, Centrale Méditerranée, FSCM, Marseille, France

*Corresponding author. E-mail: tuan-nghia.duong@univ-amu.fr

Highlights

- An approach to calibrate RF pulse of low-receptivity nuclei has been revisited
- The experimental setup and implementation is simple
- The feasibility of this approach is validated in a wide range of nuclei
- The $^{135/137}$Ba spectra of $BaTiO_3$ are recorded without prior $^{135/137}$Ba RF field calibration

Abstract

Radio-frequency (RF) field calibration is essential in NMR spectroscopy. A common practice is to collect a nutation curve by varying the pulse length in a direct single-pulse excitation experiment or in a cross-polarization magic-angle spinning with a flip-back pulse experiment. From the null points on this curve, one can calculate the RF field strength. Nevertheless, the practical implementation is not always straightforward or can even be unrealizable, especially for low-receptivity nuclei owing to their associated low sensitivity. Several researchers used an approach that involves utilizing other nuclei with more sensitivity but nearly identical Larmor frequencies to that of the nucleus of interest. However, such an approach has not been a common practice so far. In this work, we have systematically revisited this approach using 3.2 mm rotors on different sets of nuclei covering a Larmor frequency range up to 80 MHz. The effect of solid- and solution-states on RF field strength measurements has been investigated. The detection of each set of nuclei is then carried out with a resonant circuit in the NMR probe consisting of identical coils and capacitors. Our methodology is illustrated by recording $^{135/137}$Ba NMR spectra of $BaTiO_3$ without prior $^{135/137}$Ba RF field calibration.

Keywords: Nuclear magnetic resonance; RF field strength; Nutation curve; Direct single-pulse excitation method; Low-receptivity nuclei

1. Introduction

Radio-frequency (RF) pulses are fundamental in nuclear magnetic resonance (NMR) spectroscopy as they allow nuclear spins to be manipulated. Notably, proper arrangements of the RF field strength allow the selection of desired coherence pathways. For example, cross-polarization magic-angle spinning (CP MAS) [1–3] – a key experiment in solid-state NMR – involves the magnetization transfer from abundant nuclei (I) to dilute nuclei (S) for sensitivity enhancement. Such transfer occurs when the RF field strengths of both nuclei meet the Hartmann-Hahn matching condition: $|\gamma_I B_{1I} \pm \gamma_S B_{1S}| = 2\pi . n\nu_R$, where γ_X and B_{1X} denote the gyromagnetic ratio and the RF field of the X nucleus (X = I or S), respectively, whereas ν_R denotes the spinning frequency and n is an integer [4,5]. Interestingly, the use of MAS during CP experiments provides high-resolution spectra of dilute S spins by averaging out signal broadening sources, e.g chemical shift anisotropy (CSA) or ^{13}C-^{13}C dipolar couplings. However, dipolar couplings are an important source of structural information, as their magnitudes are related to spatial proximity of the coupled spins. Information on dipolar couplings or other anisotropic interactions averaged out by MAS can be selectively recovered with the help of recoupling experiments, which essentially consist of trains of RF pulses with specific values of RF field strength, phase, and pulse length. [6,7] Several popular homonuclear dipolar recoupling schemes, to name a few, are POST-C7 [8], SPC5 [9], and HORROR-based sequences [10], where the RF field strength should be calibrated to match exactly specific multiples of the spinning frequency (*i.e.* $\nu_{RF} = 7\nu_R$ for POST-C7 [8]). As a consequence, careful calibration of the RF field strength is essential for most solid-state NMR experiments.

Conventionally, RF field calibration is performed using a direct single-pulse excitation experiment – hereafter referred to as "DE" [11] (inset in Fig. 1a) – using a standard sample containing the nucleus of interest. The signal intensity of the studied nucleus is recorded as a function of the pulse length, yielding an oscillating curve whose frequency is proportional to the applied RF field strength (the so-called nutation curve). As shown in Fig. 1a, the signal is maximum when the pulse length induces a flip angle of 90° of the equilibrium longitudinal magnetization whereas it is null when the flip angle is 180° or 360°. The relation between the flip angle (θ) and the pulse length (t_p) is defined as:

$$\theta = |\gamma_X B_{1X}| t_p = 2\pi \nu_{1X} t_p \qquad (1)$$

where θ is in radians. Determination of the RF field strength is more reliable based on the pulse length corresponding to a null point (180° or 360°), as follows:

$$\nu_{1X} = \frac{\pi}{2\pi . t_{180}} = \frac{1}{2t_{180}} \text{ or } \frac{2\pi}{2\pi . t_{360}} = \frac{1}{t_{360}} \qquad (2)$$

where t_{180} and t_{360} are the pulse lengths inducing the 180° and 360° null points, respectively (red arrows in Fig. 1a). The DE method is simple but it needs to be repeated multiple times, causing long calibration times.

To avoid such repetition, Wu and Otting proposed a "one-time" method using a series of RF fields followed by a delay to sampling a data point [12]. Collecting these points also provides a nutation curve, which is then Fourier transformed to give a doublet whose splitting is twice the applied RF field strength. The ^{1}H RF field strength measured by this method was in excellent agreement with that obtained by the DE method. Nevertheless, the method proposed by Wu and Otting is recommended for RF fields associated with low power to avoid sample heating. Hence, the RF field strength at high power must be calculated and its accuracy depends on the linearity of the amplifier. Another drawback of both the DE and the "one-time" methods is that the acquisition with a sufficiently good signal-to-noise ratio (S/N) is impractical for nuclei with low natural abundance (NA), such as ^{15}N (0.36 %), ^{13}C (1.1 %) or even ^{29}Si (4.7%). Recently, Renou *et al* have reported a fast and accurate ^{13}C RF calibration at NA using MISSTEC [13]. However, this method has been limited to ^{1}H and ^{13}C solution-state NMR and is difficult to setup for solid-state NMR owing to the use of pulsed field gradients. For low NA nuclei, isotopic labeling might be an option although it increases both the cost and the complexity of the analysis.

The low sensitivity issue associated with the analysis of dilute nuclei can be partially overcome by using a CP MAS experiment followed by a "flip-back" pulse – hereafter referred to as "CP/FB" (inset in Fig. 1b). The nutation curve by CP/FB MAS is obtained by incrementing the FB pulse length. Contrary to the nutation curve in Fig. 1a, its first null point occurs when the transverse magnetization has completely returned to the z direction by a 90° pulse (red arrow in Fig. 1b) instead of a 180° or 360° pulse. Thus,

$$\nu_{1X} = \frac{\pi/2}{2\pi . t_{90}} = \frac{1}{4t_{90}} \qquad (3)$$

The CP/FB MAS experiment has the same advantages of CP MAS in terms of sensitivity enhancement, but it is still limited when studying low-receptivity nuclei. The receptivity is herein defined according to R. K. Harris as γ^3.NA.I(I + 1), where I is the spin number [14]. Moreover, in this case, fulfilling the Hartman-Hahn matching condition for CP transfer may be challenging.

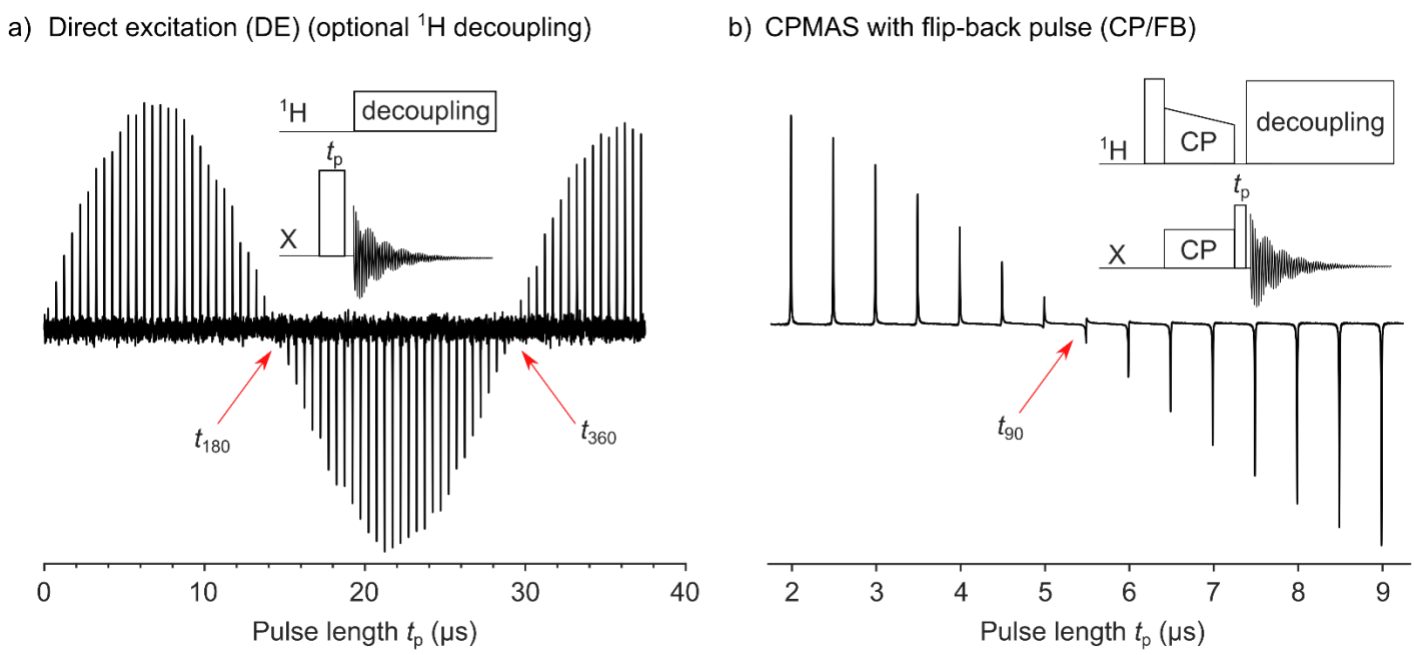

Figure 1. Nutation curve – the signal intensity as a function of pulse length – as obtained from (a) a direct excitation (DE) experiment and (b) a CP MAS with a flip-back pulse (CP/FB MAS) experiment. The null points used to measure the RF field strength are indicated by red arrows and correspond to rotation of the magnetization by (a) either 180° or 360° (t_{180} and t_{360}, respectively) or (b) 90° (t_{90}).

Hung and Gan proposed an elegant method using Bloch–Siegert shifts to calibrate the RF field strength of low-receptivity nuclei, even without their presences in the sample [15]. The sequence is identical to a TRAPDOR experiment under MAS [16]. The nutation curve of a low-receptivity nucleus is indirectly acquired through proton-detection, hereby alleviating the sensitivity issue. This method was validated by measuring ^{13}C and ^{14}N RF field strengths, which were in good agreement with CP/FB on ^{13}C and DE on ^{14}N (both under MAS), respectively. Nevertheless, the experiment is demanding because it requires very-fast MAS (≥ 60 kHz) to enhance ^{1}H resolution with prolonged T_2' relaxation time. In addition, a large first-order phase correction is needed to recover absorption mode lineshapes.

Another approach for RF field calibration on low-receptivity nuclei is to acquire nutation curves on nuclei with gyromagnetic ratios (γ) similar to that of the nucleus of interest but exhibiting higher receptivity. For example, the RF calibration for ^{14}N overtone is difficult due to its overtone nature [17–19]; however, its RF field strength has been estimated using ^{6}Li [19], ^{17}O [20], and ^{2}H nuclei [21–25]. Other examples that can be found in the literature include the use of $^{35/37}$Cl and ^{97}Mo to measure the RF field strengths of ^{61}Ni and ^{43}Ca, respectively [26–28]. For an extensive review of practical implementation of ssNMR to the study of low- γ and exotic nuclei, the reader is referred to the works of Smith, Leroy and

Bryce [29–31]. This approach is based on the fact that, for a given B_{1X}, the RF field strength is: $\nu_X(\mathrm{Hz}) = |\gamma_X . B_{1X}/2\pi|$; thus, for the same B_{1X}, similar γ_X will result in similar ν_X [32].

In this contribution, we demonstrate that the procedure proposed by Bryce *et al.* [27,28] for calibrating ^{97}Mo and ^{43}Ca RF field strengths can be extended to the study of the following 4 sets of nuclei:

- Set 1: ^{13}C, ^{23}Na, and ^{27}Al;
- Set 2: ^{29}Si and ^{127}I;
- Set 3: ^{17}O and ^{133}Cs;
- Set 4: ^{15}N and ^{35}Cl.

Importantly, the ensemble of chosen nuclei cover a vast range of Larmor frequencies (~80 MHz at 9.4 T) and each set consists of both low- and high-receptivity nuclei. We show that this approach is valid when all the nuclei belonging to the same set are analyzed using the same resonant circuit (i.e. consisting of identical coils and capacitors). We also verify that this procedure remains reliable across the whole Larmor frequency range explored as far as the Larmor frequencies of the nuclei composing each set do not differ by more than 5%. We evaluate the effect of the physical state of the sample and the experimental choice on the accuracy of RF field calibration and provide a set of standard samples adapted for calibrating the RF field strength between ~25 MHz and ~110 MHz at 9.4 T on medium sized rotors (3.2 mm outer diameter). Overall, the results show that the proposed method for calibrating the RF field strength on low-receptivity nuclei is simple, fast, and accurate (up to a couple of percent with respect to the DE method).

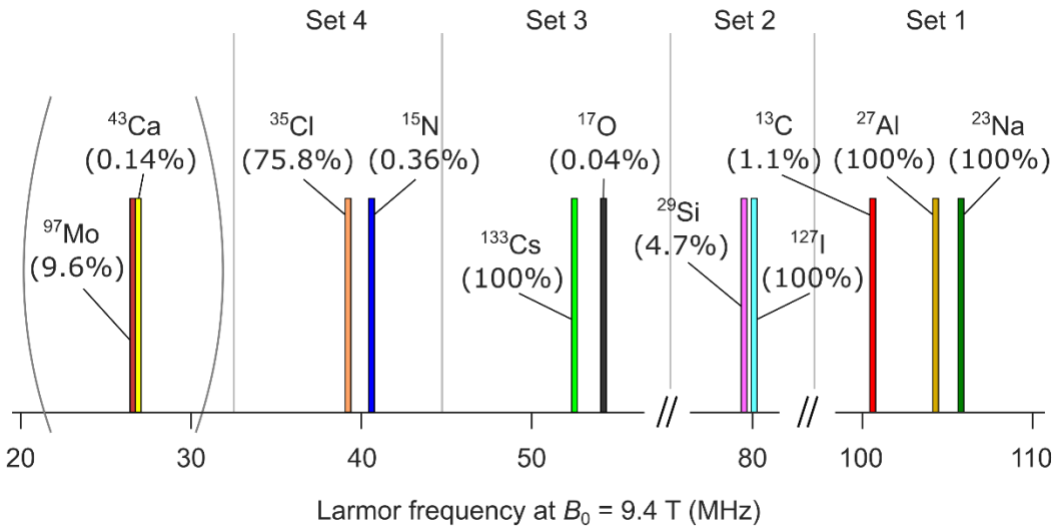

Figure 2. Nuclei studied in this work with their respective Larmor frequencies in a magnetic field of 9.4 T. Each nucleus is color coded. The number in the parentheses indicates the natural abundance (NA) of the corresponding nucleus.

2. Experimental section

Materials

1-^{13}C labeled glycine (99%), sodium trimethylsilylproranesulfonate (DSS), KI, CsCl, and ^{15}N labeled glycine (98%) were purchased from Sigma Aldrich; NaCl was purchased from Prolabo; $Al(NO_3)_3.9H_2O$ was purchased from Acros; D_2O was purchased from Merck; 62% ^{43}Ca enriched calcite was purchased from CortecNet; $Na_2MoO_4.2H_2O$ was purchased from Riedel-de Haën. ^{43}Ca enriched $CaCl_2$ solution was prepared by mixing ^{43}Ca enriched $CaCO_3$ and HCl solution. $BaTiO_3$ was synthesized according to the published procedure [33]. Samples were either used as received or used to prepare solutions with the concentrations specified in Table 1.

Solid-state NMR

For nuclei shown in Fig. 2, NMR experiments were carried out at room temperature using a 9.4 T Bruker Avance III HD spectrometer equipped with a 3.2 mm CP MAS probe operating in a double-resonance configuration. The resonant circuit in the NMR probe consists of an identical coil but different capacitors depending on the nuclei of interest. Namely, no capacitor was used for nuclei in sets 1 and 2, whereas different capacitors were used for those in sets 3 and 4, and a pair of ^{43}Ca and ^{97}Mo nuclei (but the same capacitor was used for all the nuclei of a given set and pair). Solid-state samples were analyzed with a MAS frequency of 8 kHz, whereas solution-state samples (aqueous solutions) were analyzed under static conditions. The number of scans (NS), recycling delay (RD), and the pulse sequence used for each sample are given in Table 1. The 3.2 mm sapphire rotors were used with Teflon spacers to ensure good RF field homogeneity because the variation in RF field strength at different regions within a rotor can be up to 20 – 25% [34,35], and the experiments were carried out under on-resonance conditions to avoid off-resonance effects. RF field strengths were determined at different RF powers for all the investigated nuclei: 183 W, 150 W, 120 W, 80 W, 40 W, and 20 W. The errors were calculated as: $\Delta\nu_X = \left|\frac{1}{t_{180}^{lower}} - \frac{1}{t_{180}^{upper}}\right|$ or $\left|\frac{1}{t_{360}^{lower}} - \frac{1}{t_{360}^{upper}}\right|$ for DE or $\left|\frac{1}{t_{90}^{lower}} - \frac{1}{t_{90}^{upper}}\right|$ for CP/FB, where $\Delta\nu_X$ denotes the error in measuring ν_X whereas $t_{90/180/360}^{lower/upper}$ denote the lower/upper boundary of 90°/180°/360° pulse lengths resulting in a null point.

For $^{135/137}$Ba nuclei, experiments were performed on a 9.4 T Bruker Avance III spectrometer equipped with a 4 mm standard-bore probe and at either a static condition (1M $BaCl_2$ solution) or a MAS frequency of 10 kHz ($BaTiO_3$). The 4 mm zirconia rotor was used without a spacer for sensitivity reason. For a 1M $BaCl_2$ solution, a Hahn echo was used to record ^{135}Ba NMR spectrum with the excitation and refocusing

pulse lengths of 8 and 16 μs, respectively and the echo delay was 20 μs. For $BaTiO_3$, a Hahn echo was used to record $^{135/137}$Ba NMR spectra with the excitation and refocusing pulse lengths of 4 and 8 μs, respectively and the echo delay was 96 μs. The $^{135/137}$Ba chemical shifts were referenced externally to a 1M $BaCl_2$ solution at 0 ppm. Additional experimental details are given in Table 1.

Table 1. NMR properties and NMR experimental details used for RF field strength measurements.

NMR properties						NMR experiments				
Nucleus	**Spin *I***	**NA (%)**	**γ (10^7 rad.s^{-1}.T^{-1})**	**ν_0 (MHz) at 9.4 T[a]**	**Receptivity[b]**	**Sample**	**Capaci-tors (pF)**	**Sequence**	**RD**	**NS**
^{13}C	1/2	1.1	6.728286	100.6	1.0	1-^{13}C glycine (solid)	No	CP/FB	3 s	4
								DE	10 s	1
						1M 1-^{13}C glycine		DE	10 s	1
^{23}Na	3/2	100.0	7.0808516	105.8	545	0.1M NaCl	No	DE	0.5 s	4
						1M NaCl		DE	0.5 s	1
						NaCl (solid)		DE	5 s	1
^{27}Al	5/2	100.0	6.9762780	104.3	1220	1M $Al(NO_3)_3$	No	DE	0.5 s	1
^{29}Si	1/2	4.7	-5.31903	79.5	2.2	DSS (solid)	No	CP/FB	5 s	64
^{127}I	5/2	100.0	5.38957	80.1	560	1M KI	No	DE	0.1 s	32
^{17}O	5/2	0.04	-3.62806	54.2	0.07	D_2O	18	DE	0.1 s	1024
^{133}Cs	7/2	100.0	3.533256	52.5	284	0.5 M CsCl	18	DE	5 s	4
^{15}N	1/2	0.36	-2.7126189	40.6	0.02	^{15}N glycine (solid)	43	CP/FB	3 s	4
								DE	5 s	2
						1M ^{15}N glycine		DE	15 s	8
^{35}Cl	3/2	75.8	2.6241991	39.2	21.0	1 M NaCl	43	DE	0.1 s	8
						NaCl (solid)		DE	5 s	1
^{43}Ca	7/2	0.14	-1.803069	26.9	0.05	0.3M ^{43}Ca enriched $CaCl_2$	110	DE	0.5 s	64
^{97}Mo	5/2	9.6	-1.7884	26.6	2.0	2M Na_2MoO_4	110	DE	0.5 s	64
^{135}Ba	3/2	6.6	2.677690	39.8	1.94	1M $BaCl_2$		DE	0.5 s	8192
								Hahn echo	0.1 s	6400
						$BaTiO_3$ (solid)		Hahn echo	0.5 s	4096
^{137}Ba	3/2	11.2	2.99287	44.5	4.62	$BaTiO_3$ (solid)		Hahn echo	0.5 s	4096

[a] Larmor frequency

[b] Relative receptivity normalized to natural abundance ^{13}C nucleus

3. Results and Discussions

3.1. Verification of RF field calibration of ^{43}Ca using ^{97}Mo

The acquisition of ^{43}Ca NMR spectra at NA is impractical for most samples due to its low γ and a very low NA (0.14%). Here we experimentally verify that the RF field strength of the challenging ^{43}Ca nucleus can be estimated through ^{97}Mo nucleus because their Larmor frequencies only differ by *ca.* 1%. To this aim, we obtained ^{43}Ca and ^{97}Mo nutation curves using DE experiments on aqueous solutions of $Na_2{}^{97}MoO_4$ at NA and ^{43}Ca enriched $CaCl_2$. We note that experiments were performed under the same resonance circuit consisting of identical coil and a capacitor of 110 pF. Fig. 3 shows that RF field strengths measured for ^{43}Ca and ^{97}Mo nuclei at each RF power are identical within experimental errors (*ca*. 1%), confirming the reliability of using ^{97}Mo to calibrate ^{43}Ca RF field strength, as already suggested by Bryce *et al.* [27,28].

It is worth mentioning that the RF field strength uncertainty increases with increasing RF power level. This is because higher RF powers result in larger RF field strengths, thus shorter pulse lengths to reach the null point (t_{180} or t_{360}). As mentioned in section 2, the error calculation is based on a range of pulse lengths and the pulse length is defined by the increment value. A given increment value will have a stronger effect on a shorter pulse length than on a longer one, leading to a larger error.

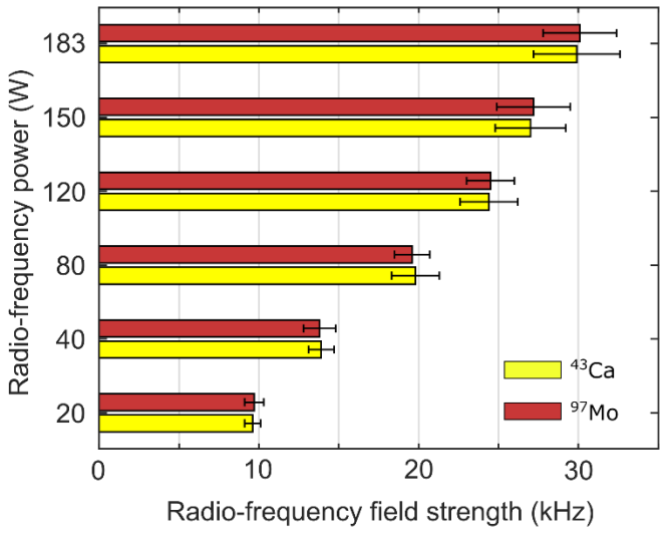

Figure 3. RF field strengths (kHz) at different applied power levels (W) for ^{43}Ca (yellow) and ^{97}Mo (brown) on ^{43}Ca enriched $CaCl_2$ and Na_2MoO_4 aqueous solutions, respectively. A resonant circuit with the same coil and capacitor of 110 pF was used.

3.2. Influence of the choice of the experiment and of the physical state of the sample on the RF field strength measurements

In the previous section, we performed the same NMR experiment (DE) on samples under the same physical states (solution). However, depending on the physical state (aqueous solution or solid powder) of the samples used to detect different nuclei investigated in this study, we will use different types of NMR experiments (DE or CP/FB MAS). Both the physical state of the sample and the choice of experiment used to acquire the nutation curve may have an impact on the measured RF field strength. Hence, in order to evaluate the possible impact of these parameters on this approach, we measured ^{13}C RF field strengths at different power levels on the same compound (1-^{13}C labeled glycine) in different physical states and using different experiments.

For 1-^{13}C labeled glycine in the solid state (as a powder), we used both DE (with ^{1}H decoupling) and CP/FB MAS experiments to collect the nutation curve, whereas for 1-^{13}C labeled glycine in an aqueous solution, we used DE (without ^{1}H decoupling) experiments. Fig. 4a shows that, within experimental errors, the obtained RF field strengths are independent on the sample preparation and experiment chosen. The same conclusion can be drawn on equivalent experiments for the measurement of RF field strengths, carried out at a lower Larmor frequency on ^{15}N nuclei. Similarly to the case of 1-^{13}C labelled glycine, we obtained nutation curves on a solid and aqueous solution of ^{15}N-labeled glycine using multiple pulse schemes (see Fig. 4b), with no noticeable difference among the measured RF field strengths.

We continued the investigations by determining the ^{23}Na RF field strength for different concentrations of NaCl solution (0.1M and 1M) and solid NaCl. Fig. 4c shows that the obtained ^{23}Na RF field strengths are almost the same no matter of the concentrations. This is different from a common knowledge that at the same RF power, the higher concentration solution will result in a weaker RF field strength than the lower one [36]. It is because the higher concentration will increase the resistance of the sample, thus reducing the efficiency of an applied RF field. An explanation for the same ^{23}Na RF field strength in Fig. 4c is possibly due to the use of moderate-size rotors (3.2 mm); hence, the resistance increase is reduced [36]. We also notice in Fig. 4c that the ^{23}Na RF field strengths for solid NaCl are systematically larger than those of 0.1M and 1M NaCl solutions but the errors are only within 3%. Nevertheless, this is not the case for ^{35}Cl since the ^{35}Cl RF field strengths for solution- and solid-state NaCl samples are identical within experimental errors as shown in Fig. 4d.

From these experiments, it is then possible to conclude that the choice of the experiment and the sample physical state do not significantly affect the RF calibrations across a vast range of Larmor frequencies.

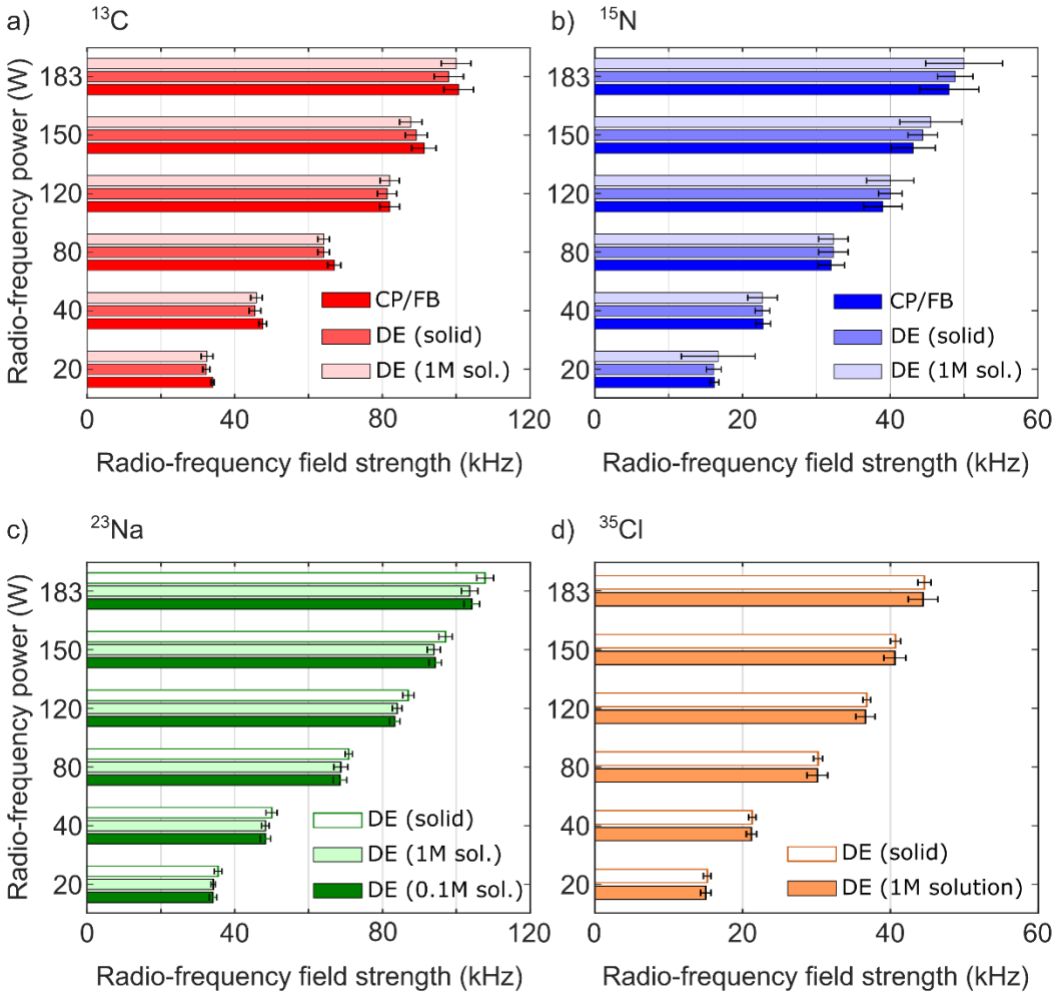

Figure 4. RF field strengths (kHz) at different applied power levels (W) for (a) ^{13}C on 1-^{13}C labeled glycine, (b) ^{15}N on ^{15}N-labeled glycine, (c) ^{23}Na and (d) ^{35}Cl on NaCl using either DE for aqueous solutions or DE and CP/FB MAS for solid-state samples.

3.3. Calibrations of RF field strengths

We examine the validity of this RF field calibration approach for set 1, composed of ^{13}C, ^{23}Na, and ^{27}Al nuclei under the same resonance circuit consisting of identical coil and capacitors. Fig. 5a shows that the RF field strengths measured for these nuclei are comparable within 4% for all the power levels used in this study. Unsurprisingly, for any given power level, RF field strengths measured for ^{13}C are systematically lower than those measured for ^{23}Na and ^{27}Al, which can be explained by considering that the Larmor frequency of ^{13}C (100.6 MHz) is slightly lower than those of ^{23}Na (105.8 MHz) and ^{27}Al (104.3 MHz) at the same magnetic field (9.4 T). This result agrees with the result from of ^{43}Ca and ^{97}Mo nuclei and shows that,

for a specific power level in a given resonant circuit, the RF field strength measured on a receptive nucleus can be used to estimate the RF field experienced by another nucleus with a Larmor frequency differing by less than 5%. In this specific case, the advantages of using ^{23}Na and ^{27}Al instead of ^{13}C are twofold: the experimental time and experimental implementation. Both ^{23}Na and ^{27}Al nuclei have a NA of 100% with spin 3/2 and 5/2, respectively; hence, their relative receptivity is 2-3 orders of magnitude larger than that of ^{13}C (Table 1), allowing much shorter experimental times. Concerning the experimental implementation, the use of ^{23}NaCl or ^{27}Al$(NO_3)_3$ aqueous solutions allows the acquisition of nutation curves by a simple DE experiment due to the complete averaging of anisotropic interactions by Brownian motions. The DE experiment avoids the need of CP optimization and ^{1}H decoupling used in CP/FB MAS.

We also investigated the validity of this approach for Set 2, composed of ^{29}Si and ^{127}I with the same resonant circuit as that used for Set 1. Fig. 5b shows that the RF field strengths measured for both nuclei at different RF powers are comparable within 6%. Another important point is that the uncertainties for ^{29}Si RF fields are much larger than those of ^{127}I because ^{29}Si NMR experiments were carried out at a relatively low NA (4.7%). As a consequence, the S/N of the ^{29}Si NMR spectra is inherently weak, notably around the zero-crossing. This increases the uncertainty in determining the null points, and hence it yields a larger uncertainty on the RF field strength determination. This is not the case for ^{127}I due to its much larger receptivity (*ca.* x250), arising from its NA of 100% and spin 5/2. Besides receptivity, similar to the ^{23}NaCl and ^{27}Al$(NO_3)_3$ cases, the use of a K^{127}I aqueous solution allows simple (and faster) DE experiments. In contrast, ^{29}Si NMR is analyzed on a solid compound (DSS), which requires the acquisition of nutation curves by CP/FB MAS experiments and hence more cumbersome experimental optimizations. It is worth noting that we can perform solution-state ^{29}Si NMR on an aqueous solution of DSS but the ^{29}Si NMR acquisition is time-consuming owing to the low NA of ^{29}Si nucleus and the absence of polarization transfer ^{1}H → ^{29}Si scheme.

Moreover, to evaluate the robustness of this approach for nuclei characterized by lower Larmor frequencies, we repeated nutation experiments on 2 additional sets of nuclear spins.

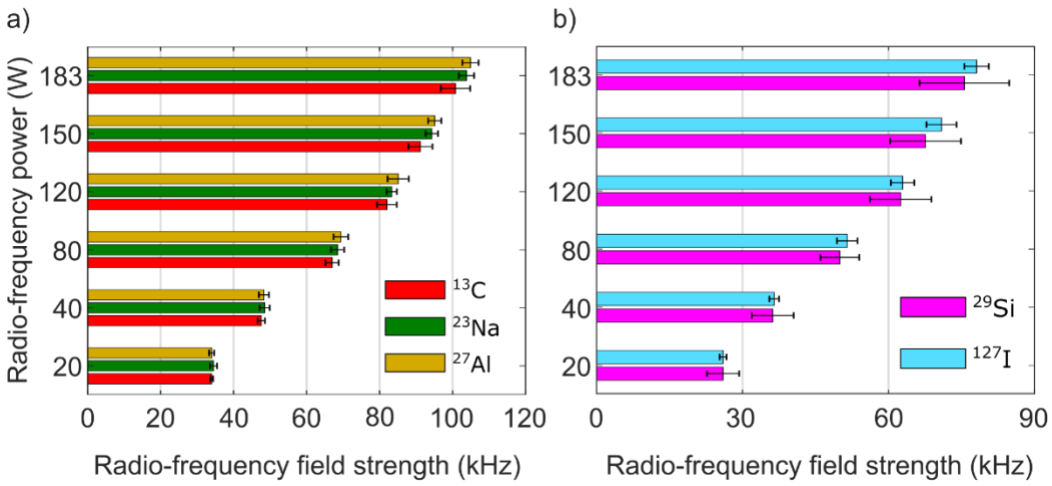

Figure 5. RF fields strengths (kHz) at different applied powers (W) for (a) ^{13}C (red), ^{23}Na (dark green), and ^{27}Al (dark yellow) as measured on 1-^{13}C labeled glycine, NaCl, and $Al(NO_3)_3$, respectively, and (b) ^{29}Si (purple) and ^{127}I (light blue) on DSS and KI, respectively. Note that the RF field strengths for ^{13}C and ^{29}Si are measured by CP/FB MAS on solids, whereas the others were measured by DE on aqueous solutions.

We tested the feasibility of the RF field calibration approach on Set 3 (^{17}O and ^{133}Cs nuclei) using the same capacitor (18 pF), and on Set 4 (^{15}N and ^{35}Cl nuclei) using the same (but different from set 3) capacitor (43 pF). Both oxygen and nitrogen atoms are ubiquitous in organic and biological compounds, but ^{17}O and ^{15}N NMR spectroscopy is challenging due to the low NA of the corresponding nuclei (0.04% and 0.36% for ^{17}O and ^{15}N, respectively), which give them extremely low receptivities (Table 1). Nevertheless, RF calibration of ^{17}O can still be carried out on natural (^{17}O) isotopic abundance D_2O within a reasonable experimental time (tens of minutes, see Table 1). Contrary to ^{17}O, the ^{15}N RF calibration requires to use an isotopically labeled ^{15}N glycine sample (or any other ^{15}N-labeled compound). To avoid the recurring problems associated with the low receptivity of ^{17}O and ^{15}N nuclei, we used ^{133}Cs and ^{35}Cl as an alternative for RF field strength calibration, respectively. This is due to the similar Larmor frequencies of each pair in Set 3 and 4 (within 3%) and the higher receptivity of ^{133}Cs and ^{35}Cl as compared to those of ^{17}O and ^{15}N. Again, aqueous solutions of ^{133}CsCl and Na^{35}Cl were prepared and simple DE experiments were recorded. Fig. 6a and 6b compare the ^{17}O and ^{15}N RF field strengths with those of ^{133}Cs and ^{35}Cl, respectively. The results show that, for each pair of nuclei (*i.e.* ^{17}O/^{133}Cs and ^{15}N/^{35}Cl), the RF field strengths at different powers are similar within 5-7%. Such deviation is sufficiently low for the so-obtained RF field strength to be used safely for recording a good quality NMR spectrum, or to be used as a reliable starting point for setting up more sophisticated (and demanding) NMR experiments. For example, $\mathrm{BR}2_2^1$ is a HORROR-based

recoupling sequence that employs the nominal RF field strength: $\nu_{RF}^{nom} = \nu_R/2$ [37–41]. We used $\mathrm{BR2}_2^1$ as an example because it involves moderate RF field strengths and relies on conventional 180° rectangular pulses (not composite pulses such as those used for POST-C7 or SPC5), which are more sensitive to RF field mismatch. Nevertheless, the simulated $\mathrm{BR2}_2^1$ double-quantum (DQ) transfer efficiency on a ^{13}C-^{13}C pair remains above 90% even when a 7% deviation from the nominal RF field strength is used (Fig. 7). We also observed that the ^{17}O and ^{15}N RF field strengths are systematically higher than the corresponding values for ^{133}Cs and ^{35}Cl (in agreement with their respectively higher Larmor frequencies).

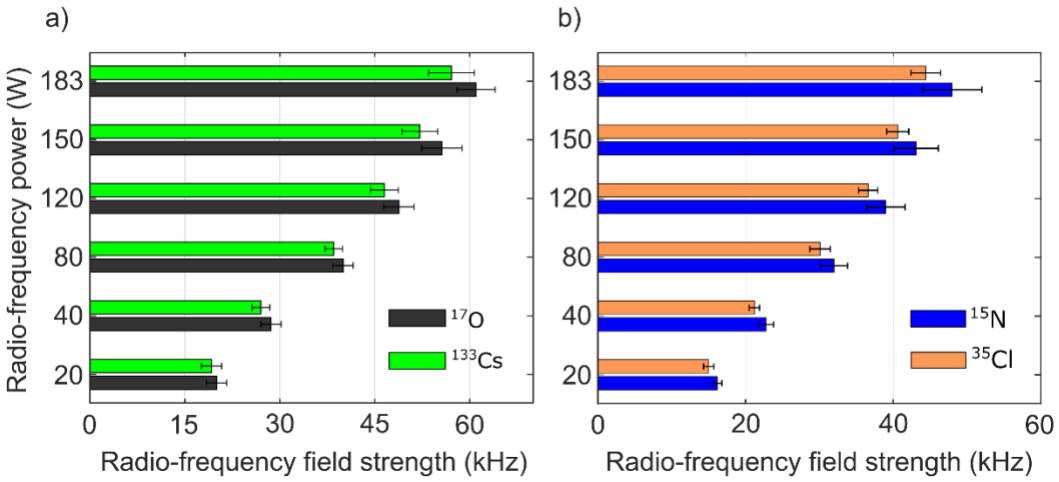

Figure 6. RF field strengths (kHz) at different applied power levels (W) for (a) ^{17}O (black) and ^{133}Cs (green) on D_2O and CsCl, respectively; (b) ^{15}N (blue) and ^{35}Cl (orange) on ^{15}N-labeled glycine and NaCl, respectively. A resonant circuit with the same coil but different capacitors for each set of nuclei was used. Note that only the RF field strength of ^{15}N was measured by CP/FB MAS, whereas the others were obtained by DE on aqueous solutions.

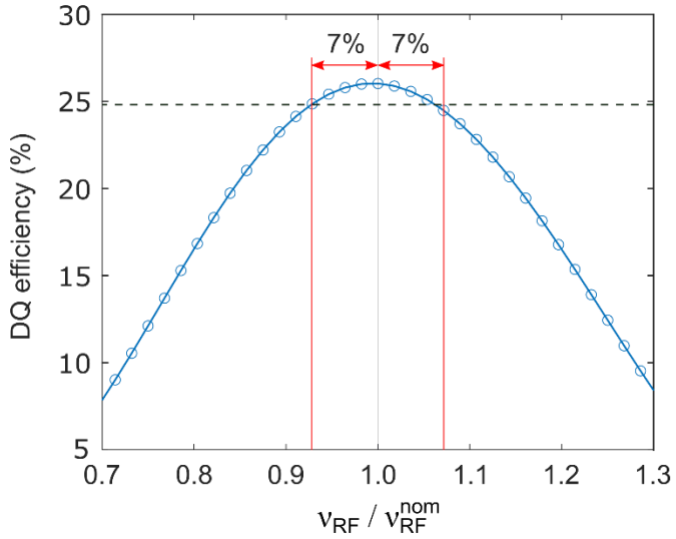

Figure 7. Plot of the simulated DQ efficiencies for $\mathrm{BR}2_2^1$ as a function of ratio between applied ν_{RF} and ν_{RF}^{nom}. Simulation was performed by SIMPSON package [42–44] on a powder of ^{13}C-^{13}C pairs at B_0 = 9.4 T with ν_R = 13.889 kHz and ν_{RF}^{nom} = 6.95 kHz and τ_{mix} = 9.2 ms. The ^{13}C-^{13}C dipolar coupling is –0.3 kHz and no aniso-/isotropic chemical shifts is considered for both ^{13}C nuclei. The starting and detecting operators are I_{1z} and $-I_{2z}$, respectively. The vertical lines indicate the deviation from the ν_{RF}^{nom} within 7% whereas the horizontal dashed line indicates the simulated DQ efficiency value at those deviations.

3.4. Application

An obvious application of estimating RF field strength is to facilitate the experimental setup. This is demonstrated by recording $^{135/137}$Ba NMR spectra of $BaTiO_3$. For experimental setup, a common practice is to prepare an aqueous solution of $BaCl_2$ for (i) chemical shift reference and (ii) $^{135/137}$Ba RF field calibration. However, this is not straightforward as the ^{135}Ba NMR spectrum of this $BaCl_2$ solution obtained using a DE experiment shows a severe rolling of the baseline (Fig. 8a), preventing the recognition of an actual ^{135}Ba peak. Such rolling has been proved due to the Ba components in the stator of the 4mm HX probe (see Figs. S1c, S2, S3c, and S4). To address this problem, a Hahn echo experiment is required because it can get rid of these additional Ba signals for a flat baseline (see Figs. S1b and S3b). However, the setup of Hahn echo experiment can be tricky when the ^{135}Ba RF field strength is not known in advance.

A solution is to use the ^{35}Cl RF field strength as an alternative due to their similar Larmor frequencies. As shown previously, ^{35}Cl RF field strength can be readily measured using NaCl solution. This approach can significantly reduce the time for experimental setup because the NA of ^{35}Cl (75.8%) is much larger than that of ^{135}Ba (6.6%) and ^{137}Ba (11.2%). Moreover, owing to its smaller quadrupolar moment, the linewidth

of ^{35}Cl is narrower than those observed for $^{135/137}$Ba, thus enhancing the corresponding S/N even further. After determination the ^{35}Cl RF field strength, we used it to record a Hahn echo experiment on a 1M $BaCl_2$ solution. A ^{135}Ba NMR spectrum free from baseline distortion was obtained, which could be readily used for chemical referencing (Fig. 8b).

We note that the ^{35}Cl RF field strength should be considered as a starting point and further optimization is still needed. According to a previous work [33], this $BaTiO_3$ sample consists of cubic and tetragonal sites, which are subject to quadrupolar interaction. Therefore, a scaling factor of $1/(I + ½) = 1/2$ (because both $^{135/137}$Ba isotopes have spin number I of 3/2) for the pulse lengths determined in solution has to be accounted for. Fig. 8c and 8d show the ^{135}Ba and ^{137}Ba Hahn echo spectra of $BaTiO_3$, respectively.

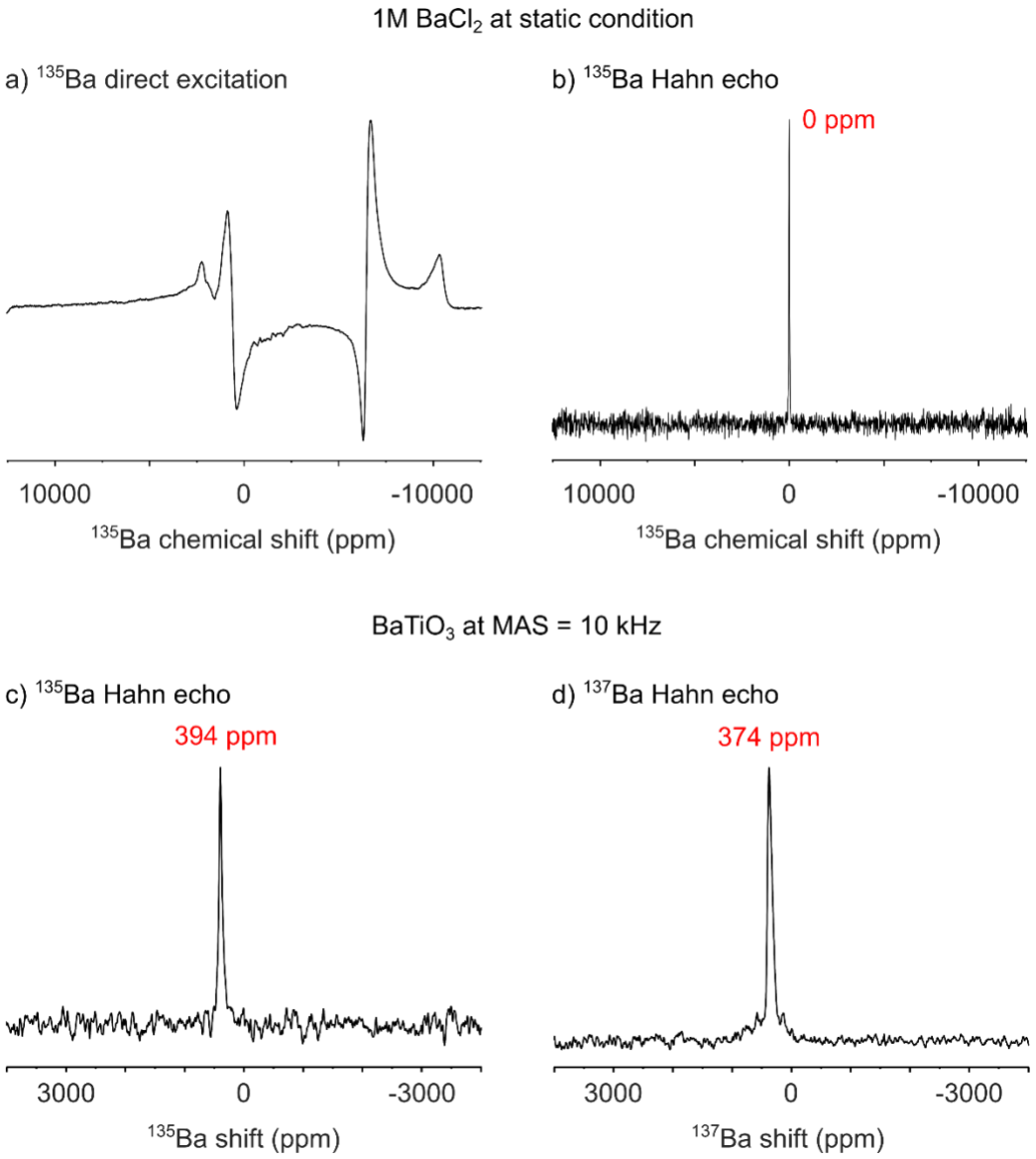

Figure 8. 1M $BaCl_2$ solution at static condition: ^{135}Ba NMR spectrum by a) DE and b) Hahn echo experiments. $BaTiO_3$ at MAS frequency of 10 kHz: c) ^{135}Ba and d) ^{137}Ba NMR spectra recorded by Hahn echo experiments.

4. Conclusion

In this work, we systematically revisited an approach to estimate the RF field strength of a low-receptivity nucleus by using other nuclei having close Larmor frequencies but with higher receptivity under the same resonant circuit. Using 3.2 mm rotors, we showed that the RF field strength of a studied nucleus is not strongly influenced by the concentration of an ionic solution, the physical state of a sample, and the choice of the experiment. The validity of this approach is confirmed on different sets of nuclei covering a range of Larmor frequencies of *ca.* 80 MHz with a RF field strength calibration error of *ca.* 7% at max. This error seems acceptable for initiating the setup of advanced NMR experiments. Other advantages of this approach are to simplify experimental calibration and to reduce experimental time. We then illustrated the method by recording $^{135/137}Ba$ NMR spectra on $BaTiO_3$ without *a priori* knowledge on $^{135/137}Ba$ RF field strengths. Finally, in this work, all RF field strengths were calibrated at ambient temperature. In the future, it would be interesting to examine the effect of temperature on RF field strength determination, which may be useful for setting up DNP MAS experiments on challenging nuclei.

Acknowledgements

This project received funding from ERC under the European Union Horizon 2020 research and innovation programme (Grant Agreement No. 758498). We thank Dr. Emanuela Callone of University of Trento for kindly providing us the $BaTiO_3$ sample.

Data availability

Data will be made available on request

References

[1] E.R.R. Andrew, A. Bradbury, R.G.G. Eades, Nuclear Magnetic Resonance Spectra from a Crystal rotated at High Speed, Nature. 182 (1958) 1659–1659. https://doi.org/10.1038/1821659a0.

[2] A. Pines, M.G. Gibby, J.S. Waugh, Proton-enhanced NMR of dilute spins in solids, J. Chem. Phys. 59 (1973) 569–590. https://doi.org/10.1063/1.1680061.

[3] J. Schaefer, E.O. Stejskal, Carbon-13 Nuclear Magnetic Resonance of Polymers Spinning at the Magic Angle, J. Am. Chem. Soc. 98 (1976) 1031–1032. https://doi.org/10.1021/ja00420a036.

[4] S.R. Hartmann, E.L. Hahn, Nuclear Double Resonance in the Rotating Frame, Phys. Rev. 128 (1962) 2042–2053. https://doi.org/10.1103/PhysRev.128.2042.

[5] E.O. Stejskal, J. Schaefer, J.S. Waugh, Magic-angle spinning and polarization transfer in proton-enhanced NMR, J. Magn. Reson. 28 (1977) 105–112. https://doi.org/10.1016/0022-2364(77)90260-8.

[6] M.H. Levitt, Symmetry-Based Pulse Sequences in Magic-Angle Spinning Solid-State NMR, EMagRes. 9 (2007) 165–196. https://doi.org/10.1002/9780470034590.

[7] M. Eden, Advances in symmetry-based pulse sequences in magic-angle spinning solid-state NMR, EMagRes. 2 (2013) 351–364. https://doi.org/10.1002/9780470034590.emrstm1326.

[8] M. Hohwy, H.J. Jakobsen, M. Edén, M.H. Levitt, N.C. Nielsen, Broadband dipolar recoupling in the nuclear magnetic resonance of rotating solids: A compensated C7 pulse sequence, J. Chem. Phys. 108 (1998) 2686–2694. https://doi.org/10.1063/1.475661.

[9] M. Hohwy, C.M. Rienstra, C.P. Jaroniec, R.G. Griffin, Fivefold symmetric homonuclear dipolar recoupling in rotating solids: Application to double quantum spectroscopy, J. Chem. Phys. 110 (1999) 7983. https://doi.org/10.1063/1.478702.

[10] N.C. Nielsen, H. Bildsøe, H.J. Jakobsen, M.H. Levitt, Double-quantum homonuclear rotary resonance: Efficient dipolar recovery in magic-angle spinning nuclear magnetic resonance, J. Chem. Phys. 101 (1994) 1805–1812. https://doi.org/10.1063/1.467759.

[11] P.A. Keifer, 90° pulse width calibrations: How to read a pulse width array, Concepts Magn. Reson. 11 (1999) 165–180. https://doi.org/10.1002/(SICI)1099-0534(1999)11:3<165::AID-CMR4>3.0.CO;2-D.

[12] P.S.C. Wu, G. Otting, Rapid pulse length determination in high-resolution NMR, J. Magn. Reson. 176 (2005) 115–119. https://doi.org/10.1016/j.jmr.2005.05.018.

[13] S. Renou, J. Pontabry, G. Assemat, S. Akoka, Radio-frequency pulse calibration using the MISSTEC sequence, J. Magn. Reson. 341 (2022). https://doi.org/10.1016/j.jmr.2022.107260.

[14] R.K. Harris, N.m.r. and the periodic table, Chem. Soc. Rev. 5 (1976) 1. https://doi.org/10.1039/cs9760500001.

[15] I. Hung, P. Gor'kov, Z. Gan, Using the heteronuclear Bloch-Siegert shift of protons for B_1 calibration of insensitive nuclei not present in the sample, J. Magn. Reson. 310 (2020) 106636. https://doi.org/10.1016/j.jmr.2019.106636.

[16] C.P. Grey, A.J. Vega, Determination of the Quadrupole Coupling Constant of the Invisible Aluminum Spins in Zeolite HY with $^{1}H/^{27}Al$ TRAPDOR NMR, J. Am. Chem. Soc. 117 (1995) 8232–8242. https://doi.org/10.1021/ja00136a022.

[17] M. Bloom, M.A. LeGros, Direct detection of two-quantum coherence, Can. J. Phys. 64 (1986) 1522–1528. https://doi.org/10.1139/p86-271.

[18] R. Tycko, S.J. Opella, High-Resolution ^{14}N Overtone Spectroscopy: An Approach to Natural Abundance Nitrogen NMR of Oriented and Polycrystalline Systems, J. Am. Chem. Soc. 108 (1986) 3531–3532. https://doi.org/10.1021/ja00272a071.

[19] R. Tycko, S.J. Opella, Overtone NMR spectroscopy, J. Chem. Phys. 86 (1987) 1761. https://doi.org/10.1063/1.452176.

[20] I.M. Haies, J.A. Jarvis, L.J. Brown, I. Kuprov, P.T.F. Williamson, M. Carravetta, ^{14}N overtone transition in double rotation solid-state NMR, Phys. Chem. Chem. Phys. 17 (2015) 23748–23753. https://doi.org/10.1039/C5CP03266K.

[21] L.A. O'Dell, C.I. Ratcliffe, ^{14}N magic angle spinning overtone NMR spectra, Chem. Phys. Lett. 514 (2011) 168–173. https://doi.org/10.1016/j.cplett.2011.08.030.

[22] L. O'Dell, R. He, J. Pandohee, Identifying H–N proximities in solid-state NMR using ^{14}N overtone irradiation under fast MAS, CrystEngComm. 15 (2013) 8657–8667. https://doi.org/10.1039/c3ce40967h.

[23] Y. Nishiyama, M. Malon, Z. Gan, Y. Endo, T. Nemoto, Proton-nitrogen-14 overtone two-dimensional correlation NMR spectroscopy of solid-sample at very fast magic angle sample spinning., J. Magn. Reson. 230 (2013) 160–4. https://doi.org/10.1016/j.jmr.2013.02.015.

[24] L.A. O'Dell, A. Brinkmann, ^{14}N overtone NMR spectra under magic angle spinning: Experiments and numerically exact simulations, J. Chem. Phys. 138 (2013). https://doi.org/10.1063/1.4775592.

[25] L. O'Dell, ^{14}N Overtone Magic Angle Spinning NMR, Annu. Reports NMR Spectrosc. 86 (2015) 211–236. https://doi.org/10.1016/bs.arnmr.2015.04.003.

[26] P. Werhun, D.L. Bryce, Structural and Crystallographic Information from ^{61}Ni Solid-State NMR Spectroscopy: Diamagnetic Nickel Compounds, Inorg. Chem. 56 (2017) 9996–10006.

https://doi.org/10.1021/acs.inorgchem.7b01536.

[27] K.M.N. Burgess, F.A. Perras, I.L. Moudrakovski, Y. Xu, D.L. Bryce, High sensitivity and resolution in ^{43}Ca solid-state NMR experiments, Can. J. Chem. 93 (2015) 799–807. https://doi.org/10.1139/cjc-2014-0528.

[28] K.M.N. Burgess, D.L. Bryce, On the crystal structure of the vaterite polymorph of CaCO3: A calcium-43 solid-state NMR and computational assessment, Solid State Nucl. Magn. Reson. 65 (2015) 75–83. https://doi.org/10.1016/j.ssnmr.2014.08.003.

[29] M.E. Smith, Low-γ Nuclei in Solid Samples, EMagRes. 2007 (2007). https://doi.org/10.1002/9780470034590.emrstm0278.

[30] C. Leroy, D.L. Bryce, Recent Advances in Solid-State Nuclear Magnetic Resonance Spectroscopy of Exotic Nuclei, Prog. Nucl. Magn. Reson. Spectrosc. (2018). https://doi.org/10.1016/j.pnmrs.2018.08.002.

[31] M.E. Smith, Recent progress in solid-state NMR of spin-½ low-γ nuclei applied to inorganic materials, Phys. Chem. Chem. Phys. 25 (2022) 26–47. https://doi.org/10.1039/d2cp03663k.

[32] E. Fukushima, S.B.W. Roeder, Experimental Pulse NMR A Nuts and Bolts Approach, CRC Press, 1981. https://doi.org/10.1201/9780429493867.

[33] N. Zamperlin, R. Ceccato, M. Fontana, A. Pegoretti, A. Chiappini, S. Dirè, Effect of hydrothermal treatment and doping on the microstructural features of sol-gel derived $BaTiO_3$ nanoparticles, Materials (Basel). 14 (2021). https://doi.org/10.3390/ma14154345.

[34] Z. Tošner, A. Purea, J.O. Struppe, S. Wegner, F. Engelke, S.J. Glaser, B. Reif, Radiofrequency fields in MAS solid state NMR probes, J. Magn. Reson. 284 (2017) 20–32. https://doi.org/10.1016/j.jmr.2017.09.002.

[35] H. Nagashima, J. Trébosc, O. Lafon, F. Pourpoint, P. Paluch, M.J. Potrzebowski, J.P. Amoureux, Imaging the spatial distribution of radiofrequency field, sample and temperature in MAS NMR rotor, Solid State Nucl. Magn. Reson. 87 (2017) 137–142. https://doi.org/10.1016/j.ssnmr.2017.08.001.

[36] M.W. Voehler, G. Collier, J.K. Young, M.P. Stone, M.W. Germann, Performance of cryogenic probes as a function of ionic strength and sample tube geometry, J. Magn. Reson. 183 (2006) 102–109. https://doi.org/10.1016/j.jmr.2006.08.002.

[37] B. Hu, Q. Wang, O. Lafon, J. Trébosc, F. Deng, J.P. Amoureux, Robust and efficient spin-locked symmetry-based double-quantum homonuclear dipolar recoupling for probing (1)H-(1)H proximity in the solid-state., J. Magn. Reson. 198 (2009) 41–8. https://doi.org/10.1016/j.jmr.2009.01.002.

[38] B. Hu, L. Delevoye, O. Lafon, J. Trébosc, J.P. Amoureux, Double-quantum NMR spectroscopy of ^{31}P species submitted to very large CSAs., J. Magn. Reson. 200 (2009) 178–88. https://doi.org/10.1016/j.jmr.2009.06.020.

[39] Q. Wang, B. Hu, O. Lafon, J. Trébosc, F. Deng, J.P. Amoureux, Double-quantum homonuclear NMR correlation spectroscopy of quadrupolar nuclei subjected to magic-angle spinning and high magnetic field, J. Magn. Reson. 200 (2009) 251–260. https://doi.org/10.1016/j.jmr.2009.07.009.

[40] Q. Wang, B. Hu, F. Fayon, J. Trébosc, C. Legein, O. Lafon, F. Deng, J.-P. Amoureux, Double-quantum ^{19}F-^{19}F dipolar recoupling at ultra-fast magic angle spinning NMR: application to the assignment of ^{19}F NMR spectra of inorganic fluorides., Phys. Chem. Chem. Phys. 11 (2009) 10391–10395. https://doi.org/10.1039/b914468d.

[41] N.T. Duong, D. Lee, F. Mentink-Vigier, O. Lafon, G. De Paëpe, On the use of radio-frequency offsets for improving double-quantum homonuclear dipolar recoupling of half-integer-spin quadrupolar nuclei, Magn. Reson. Chem. 59 (2021) 991–1008. https://doi.org/10.1002/mrc.5142.

[42] M. Bak, J.T. Rasmussen, N.C. Nielsen, SIMPSON: a general simulation program for solid-state NMR spectroscopy., J. Magn. Reson. 147 (2000) 296–330. https://doi.org/10.1016/j.jmr.2011.09.008.

[43] Z. Tošner, R. Andersen, B. Stevensson, M. Edén, N.C. Nielsen, T. Vosegaard, Computer-intensive simulation of solid-state NMR experiments using SIMPSON, J. Magn. Reson. 246 (2014) 79–93. https://doi.org/http://dx.doi.org/10.1016/j.jmr.2014.07.002.

[44] D.W. Juhl, Z. Tošner, T. Vosegaard, Versatile NMR simulations using SIMPSON, Annu. Reports NMR Spectrosc. 100 (2020) 1–59. https://doi.org/10.1016/bs.arnmr.2019.12.001.

SUPPORTING INFORMATION

A facile approach for estimating radio-frequency field strength of low-receptivity nuclei

Nghia Tuan Duong[a]*, Stéphane Viel[a,b], Fabio Ziarelli[c], Pierre Thureau[a], and Giulia Mollica[a]

[a] Aix Marseille Univ, CNRS, ICR, Marseille, France

[b] Institut Universitaire de France, Paris, France

[c] Aix Marseille Univ, CNRS, Centrale Méditerranée, FSCM, Marseille, France

*Corresponding author. E-mail : tuan-nghia.duong@univ-amu.fr

In order to understand the origin of the severe rolling of the baseline in Fig. 8a, we performed ^{135}Ba experiments when no rotor, thus no sample was inserted. The similarity of ^{135}Ba spectra in Fig. S1c and S1d clearly shows that the cause of such rolling is from the probe, not the sample. We note here that the ^{135}Ba spectra in Fig. S1d and Fig. 8a are obtained from the identical experiment but are differently phased.

We continued to perform ^{135}Ba experiments when no rotor was inserted but at a different pulse length and an offset to identify if the rolling is due to the probe ringing. The spectra in Fig. S2 are different, demonstrating that the severe rolling of the baseline in Fig. 8a comes from the Ba components in the stator of the 4mm HX probe.

We had to use Hahn echo experiments to average such interfering ^{135}Ba signals (see Fig. S1c), which was difficult to setup without the prior knowledge on ^{135}Ba RF field strength.

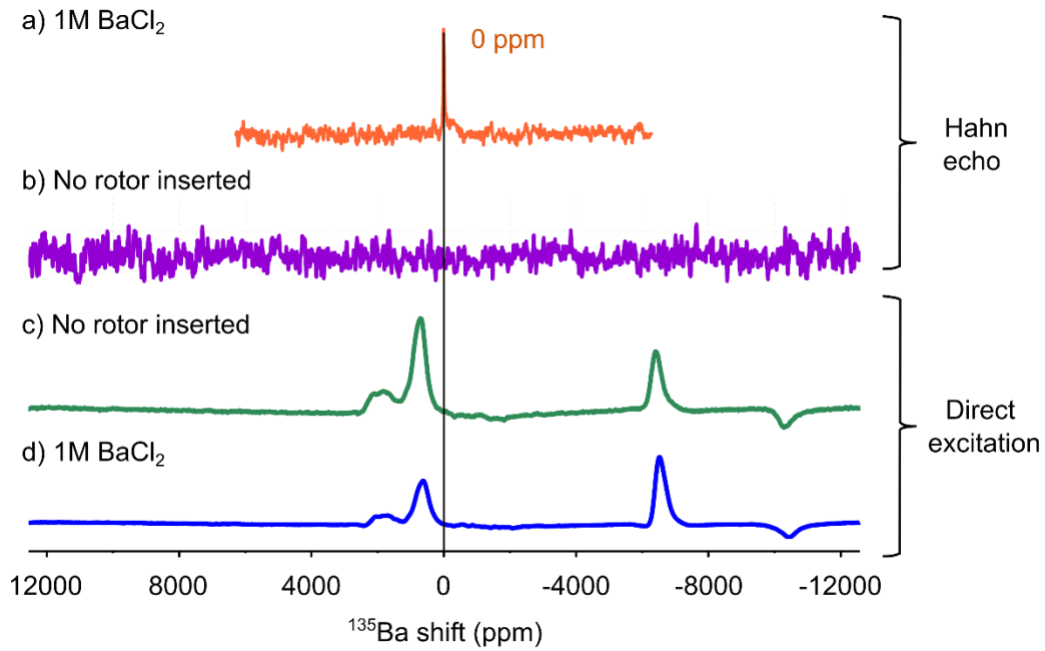

Figure S1. ^{135}Ba spectra of a (a,d) 1M $BaCl_2$ solution and (b,c) blank sample when no rotor was inserted obtained under (a,b) Hahn echo and (c,d) direct single-pulse experiments.

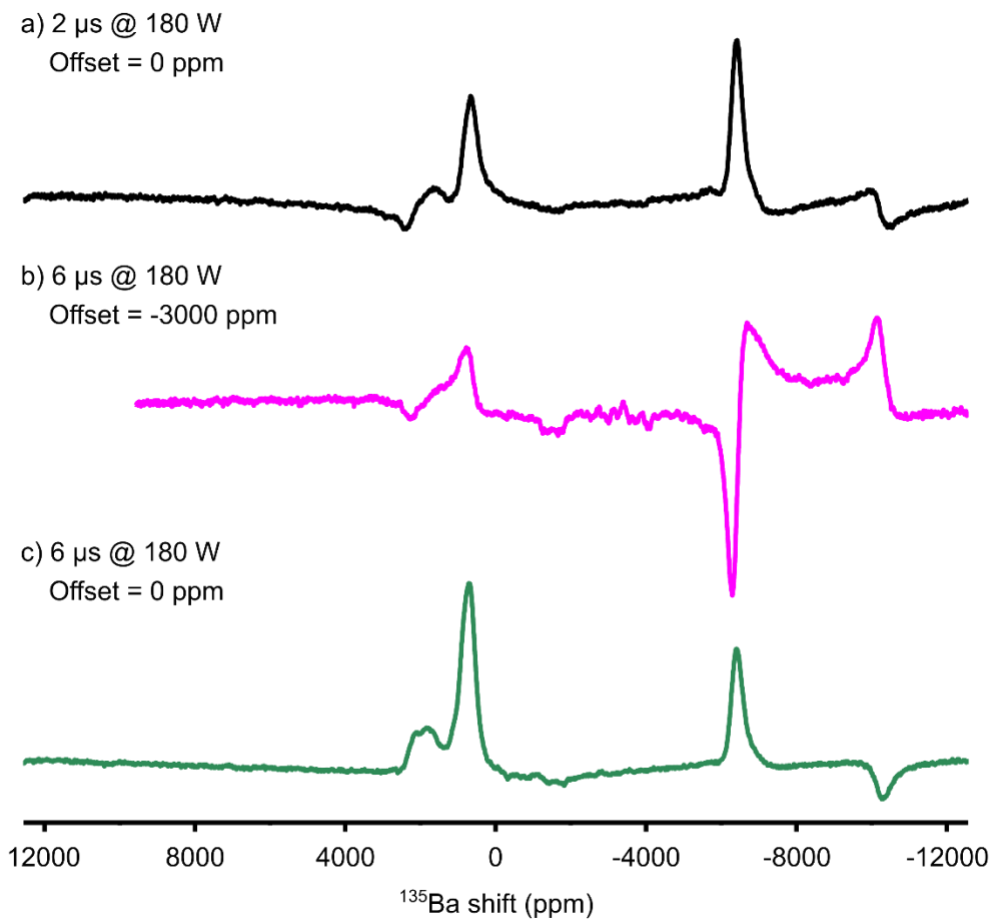

Figure S2. ^{135}Ba spectra of a blank sample when no rotor was inserted obtained under a single-pulse experiment at (a) a pulse length of 2 µs and offset of 0 ppm, (a) a pulse length of 6 µs and offset of -3000 ppm, and (c) a pulse length of 6 µs and offset of 0 ppm.

An identical set of ^{137}Ba experiments was also performed to validate the presence of Ba components (Fig. S3c and S3d, Fig. S4) in the stator of the 4mm HX probe. The Hahn echo was a must to remove these ^{137}Ba signals for a flat baseline (see Fig. S3b).

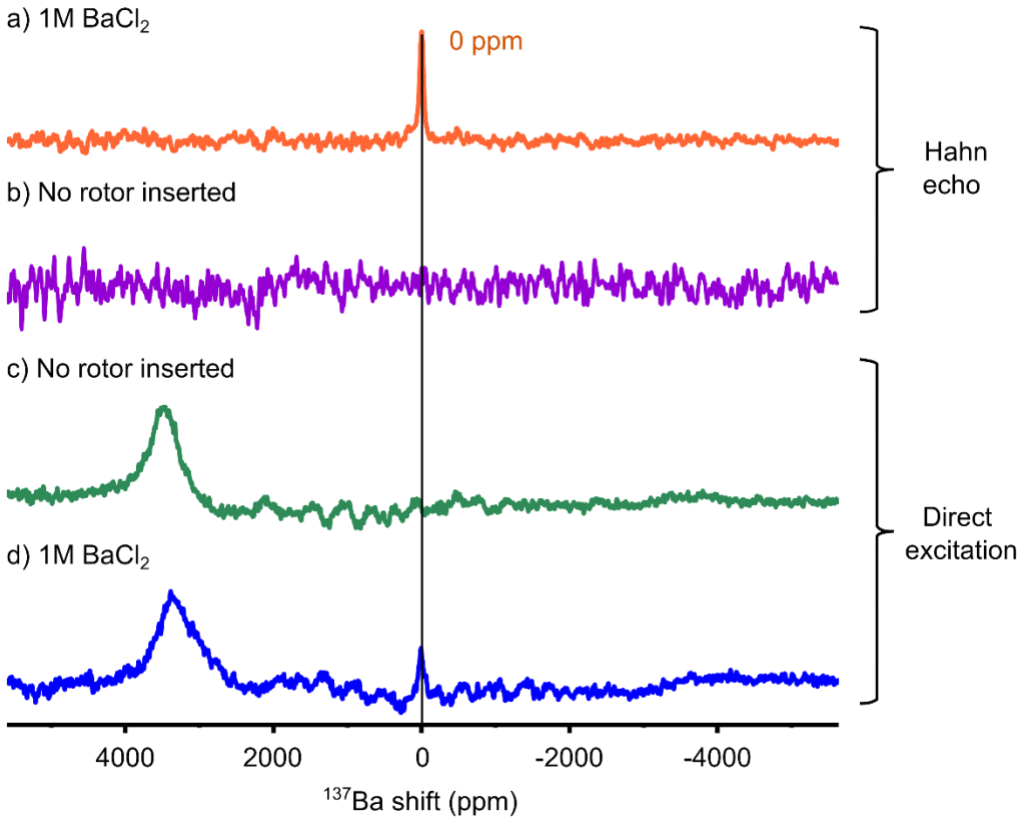

Figure S3. ^{137}Ba spectra of a (a,d) 1M $BaCl_2$ solution and (b,c) blank sample when no rotor was inserted obtained under (a,b) Hahn echo and (c,d) direct single-pulse experiments.

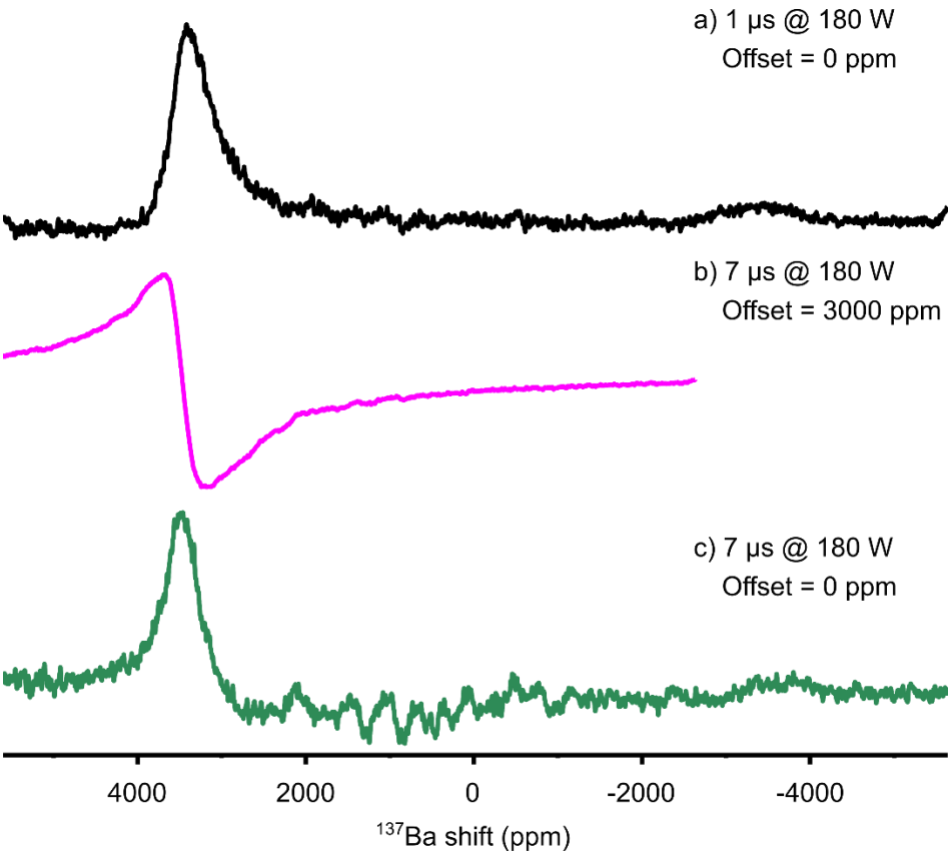

Figure S4. ^{137}Ba spectra of a blank sample when no rotor was inserted obtained under a single-pulse experiment at (a) a pulse length of 1 µs and offset of 0 ppm, (a) a pulse length of 7 µs and offset of 3000 ppm, and (c) a pulse length of 7 µs and offset of 0 ppm.